

---

# Improving Performance of Spike-based Deep Q-Learning using Ternary Neurons

---

Aref Ghoreishee, Abhishek Mishra, John Walsh, Anup Das, Nagarajan Kandasamy  
Electrical and Computer Engineering Department  
Drexel University  
Philadelphia, PA 19104  
{ag4247, am4862, jmw96, ad3639, kandasamy}@drexel.edu

## Abstract

We propose a new ternary spiking neuron model to improve the representation capacity of binary spiking neurons in deep Q-learning. Although a ternary neuron model has recently been introduced to overcome the limited representation capacity offered by the binary spiking neurons, we show that its performance is worse than that of binary models in deep Q-learning tasks. We hypothesize gradient estimation bias during the training process as the underlying potential cause through mathematical and empirical analysis. We propose a novel ternary spiking neuron model to mitigate this issue by reducing the estimation bias. We use the proposed ternary spiking neuron as the fundamental computing unit in a deep spiking Q-learning network (DSQN) and evaluate the network's performance in seven Atari games from the Gym environment. Results show that the proposed ternary spiking neuron mitigates the drastic performance degradation of ternary neurons in Q-learning tasks and improves the network performance compared to the existing binary neurons, making DSQN a more practical solution for on-board autonomous decision-making tasks.

## 1 Introduction

Reinforcement learning (RL) algorithms, such as Q-learning, when used in mobile and autonomous systems, such as robots and drones, enable them to learn complex decision-making strategies in dynamic and uncertain operating environments. The onboard processing of these algorithms on mobile systems allows for faster responses, reduced latency, and the ability to operate in remote or communication-limited environments. In addition, power is the leading design constraint in many such platforms, and the impact of hardware and software design decisions on mission performance, endurance, and reliability must be considered early in the design cycle.

Deep reinforcement learning (DRL) has shown impressive results in decision making in numerous application domains, including autonomous vehicle and robot navigation in dynamic environments [1–4]. However, the power consumed by DRL-based algorithms, especially those developed using classical deep neural networks (DNNs) such as deep Q networks (DQN), during inference can be a limiting factor in their deployment on mobile platforms [5]. *Spiking neural networks (SNNs)* offer a promising pathway to accomplish this task. These networks are inspired by the operational principles of biological neurons, in which neurons communicate with each other by sending short impulses, called spikes, through synapses. Such spiking neurons can be organized into feed-forward layers or in a recurrent topology [6, 7]. This form of brain-inspired computing holds significant promise for various spatial and temporal pattern recognition tasks [8–11].

SNN offers a much simpler computational model compared to a traditional artificial neural network (ANN) due to two main reasons: spike activity within the SNN is typically sparse, with many

neurons inactive at any given moment, leading to fewer active calculations; and addition operations dominate over multiplication operations [12, 13]. Together, these features create an extremely energy-efficient processing paradigm. SNNs can be deployed on neuromorphic chips designed specifically to execute them [14]. Several designs have been developed; for example, DYNAPSE [15], Loihi [16], Akida [17], and TrueNorth [18]. Various FPGA-based architectures have also recently been developed [19–24].

The inherent computational efficiency of SNNs has motivated the development of deep spiking reinforcement learning networks such as *deep spiking Q networks (DSQN)* in which classical neurons are replaced by leaky integrate and fire (LIF) spiking neurons that produce binary outputs (0 or 1) in a predefined simulation time window [25, 26]. However, SNNs currently lag behind their more traditional counterparts in terms of performance capabilities for two main reasons. First, the non-differentiable nature of spiking neurons complicates training. Common approaches to address this issue include converting trained classical ANNs into their SNN variants [27, 28], and using surrogate gradient learning [29, 30], where surrogate gradients are used during backpropagation to estimate the gradient of spike generation. The conversion-based approach shows poorer performance compared to the original ANN and requires large simulation time windows, increasing energy cost and inference latency [27]. The use of surrogate gradients is more popular because it generally results in better performance [25]. Spiking neurons typically encode information using binary values  $\{0, 1\}$ , which inherently limits their representation capacity. This is a more significant limitation and, in fact, SNNs suffer from lower performance in complex and high-dimensional environments [26]. Some approaches have been proposed to mitigate this problem, focusing on spike encoding [26], but the computationally demanding nature of the solutions and the necessity to implement the encoding layer outside the neuromorphic chip make this approach inefficient.

Recently, a ternary spiking neuron model that can produce three values,  $\{-1, 0, 1\}$ , has been introduced to improve the limited representation capacity of the spiking neuron [31]. This model can be useful for describing more complex neural behaviors, such as where the inhibitory (-1) and excitatory (+1) inputs interact dynamically within the SNN, and has been used to build SNNs for computer vision and natural language processing tasks with promising results [31, 32]. The SNN requires 2-bit activations per neuron that incur slightly more processing (and energy) overhead. However, no additional multiplication operations are introduced.

*This paper presents the first evaluation of ternary neuron-based SNNs within the deep Q-learning framework, investigating their potential to address the limited representation capacity of conventional binary neuron-based SNNs for reinforcement learning tasks.* Towards this end, our key contributions and findings can be summarized as follows.

- We mathematically analyze the representation capacity and training dynamics of ternary SNNs and show that there is a trade-off between maximizing the representation capacity and minimizing the gradient estimation bias during training.
- Reducing gradient estimation bias is important for RL tasks, since the quality of training data in the replay buffer relies on the training dynamics of the RL agent. Toward this goal, and inspired by the behavior of biological neurons, we propose a novel ternary spiking neuron model with asymmetric thresholds for producing positive and negative spikes.
- We show that DSQNs that use our proposed ternary neuron model, called *Deep Asymmetric Ternary Spiking Q-Networks (DATSQN)*, exhibit stable training behavior, using the concept of dynamic isometry [32, 33]. We define stability as the ability to prevent both the vanishing and exploding gradient problems.

DATSQN is evaluated on seven Atari games from the Gym environment, using the binary spiking neuron-based SNN architecture from [29] as a baseline. To enable fully spiking computation, compatible with neuromorphic hardware, we encode raw pixel input into spike trains using rate-based Bernoulli sampling, unlike [29], which processes raw pixels directly, resulting in a non-spiking first layer with floating-point operations. To further challenge the agents while reducing latency and energy consumption, we also used a simulation time window shorter than the baseline. Under these more neuromorphic-friendly conditions, DATSQN achieves a 30% improvement in performance.

The paper is organized as follows. Section 2 discusses related work. Section 3 provides the necessary background on deep Q-learning networks and their spiking variants. Section 4 describes our overall

methodology that led to the development of DATSQN. Section 5 presents the key results, and we conclude the paper in Section 6.

## 2 Related Work

Brain-inspired computing has the potential to process information with extreme energy efficiency and deal with unstructured and noisy data [34]. As a brain-inspired computing approach, SNNs can potentially make deep learning extremely energy efficient [35]. SNNs can be implemented on neuromorphic chips [36] and due to the event-driven nature of SNNs, their energy consumption will be ten to hundreds of mW [37].

Although previous work has focused on the use of SNNs for computer vision tasks [38–41], their use in more complex tasks such as language modeling [32, 42, 43] and reinforcement learning (RL) [25, 44] has recently been studied, resulting in increased attention paid to the limited representation capacity of binary spiking neurons [31, 32, 45]. This motivated the ternary spiking neuron model.

DRL is a combination of ANN and RL [34]. The first DRL algorithm was introduced by combining Q learning, a traditional RL algorithm, and an ANN named DQN [35]. Mnih et al. improved the performance of the original DQN, developing practical solutions such as a replay buffer and  $\epsilon$ -greedy method [36]. A double DQN was proposed to solve the problem of overestimation [37], the concept of dueling DQNs has been used to improve the stability of the base network [38], and the concepts behind double and dueling DQNs have also been integrated [39].

The high energy consumed by DRL algorithms motivated the introduction of the first DSQN, converting a pre-trained DQN into a DSQN [28], which, however, led to lower performance compared to the DQN. An improved conversion approach proposed by Tan et al. requires a larger simulation time window, leading to increased latency and energy consumption [40]. To mitigate these issues, training of DSQNs using pseudo-gradients was developed [29]. Sun et al. propose a batch normalization approach for DSQN, at the expense of incurring additional computation within the network [41]. The impact of tuning various hyper-parameters on DSQN performance has also been studied [25, 42]. Although these efforts have made DSQN a promising solution, its effectiveness when applied to complex, high-dimensional tasks diminishes because of the limited representation capacity of binary spiking neurons, which becomes even more severe when smaller simulation-time windows are used to reduce latency in time-critical tasks.

Our work explores the practicality of using ternary spiking neurons to enhance the representational capacity of DSQNs. Our findings reveal that existing ternary spiking neurons degrade the performance of DSQNs, even compared to binary spiking neurons. To solve this issue, we propose a novel asymmetric ternary spiking model, which can also be applied to other applications of SNNs. Given the critical importance of training stability, we also show that networks containing asymmetric ternary spiking neurons exhibit high training stability.

## 3 Preliminaries

Consider a task in which an agent interacts with an environment through a sequence of actions, observations, and rewards. At each time step  $t$ , the agent selects an action from a set of possible actions  $\mathcal{A} = \{a_1, \dots, a_k\}$  and applies it to the environment. The agent receives a reward  $r_t$ , and observes the new state of the environment  $s_t \in S$ . It is impossible for the agent to fully capture the state of the environment and therefore relies only on its observation, denoted by  $s_t$ . The assumption here is that the underlying process is a Markov decision process, which means that the state at time  $t$  depends on the state  $s_{t-1}$  and the action  $a_{t-1}$  taken by the agent at the previous time step. Assuming that future rewards are discounted by a factor of  $\lambda$  per time step, the future cumulative discounted rewards at time  $t$ , called return, are  $R_t = \sum_{i=t}^T \lambda^{i-t} r_i$  where  $T$  is the time step at which the interaction ends. The optimal action-value function is the maximum return achievable by following any policy and is given as

$$Q^*(s, a) = \mathbb{E} \left[ r + \lambda \max_{a' \in \mathcal{A}} Q(s', a'), \mid s, a \right], \quad (1)$$

where  $s'$  is the state obtained after taking action  $a$  by the agent. The idea of DQN is to approximate  $Q^*(s, a)$  using a deep neural network. Due to the correlations between the action-value function,  $Q^*(s, a)$ , and the target values,  $r + \lambda \max_{a' \in \mathcal{A}} Q(s', a')$ , the learning algorithm becomes unstable. Mnih et al. propose an iterative update algorithm which adjusts the action-value function towards

target values that are only periodically updated, resulting in a stable training process [36]. This algorithm has been adopted by several subsequent advances in DQN [37, 43–47].

A DSQN can be established by substituting neurons in a DQN with spiking neurons, such as the LIF [48] or Izhikevich [7] neuron models. These neurons encode information within the network into spike sequences. Due to simpler hardware implementation and high flexibility, LIF neurons are more popular and have been used in many works within the SNN domain [49–53]. LIF neurons encode information as a sequence of 0 or 1 over a simulation time window, and we refer to them as binary LIF neurons in this work.

**Binary LIF Neuron Model.** The dynamics, described by Equation (2), simulate the charging and firing of biological neurons [31, 32]. Here,  $t \in \mathcal{T}$  denotes the time step where the binary LIF neuron performs spike encoding over a predefined time duration  $\mathcal{T}$  called simulation time window,  $m^l(t)$  and  $v^l(t)$  are the membrane potentials of the neuron in layer  $l$  before and after a possible spike emission, respectively, and  $v^{\text{th}}$ ,  $\beta$ , and  $v_{\text{reset}}$  represent the firing threshold, the decay factor, and the reset potential of the membrane, respectively. The underlying idea is as follows: the neuron in layer  $l$  receives the input from the previous layer,  $x^{(l-1)}(t)$ , and the membrane potential of the neuron updates to  $m^l(t)$ . Then, if the updated membrane potential,  $m^l(t)$ , is greater than  $v^{\text{th}}$ , the output of the neuron is 1 (spike); otherwise, the output is 0 (no spike). If a spike is generated, the membrane potential will reset to the predefined  $v_{\text{reset}}$ ; otherwise, the membrane potential will decay by a factor denoted by  $\beta$ .

$$\begin{aligned} m^l(t) &= v^l(t-1) + x^{l-1}(t) \\ s^l(t) &= \begin{cases} 0 & \text{if } m^l(t) < v^{\text{th}} \\ 1 & \text{if } m^l(t) \geq v^{\text{th}} \end{cases} \\ v^l(t) &= \beta m^l(t)(1 - s^l(t)) + v_{\text{reset}} s^l(t) \end{aligned} \quad (2)$$

In the above encoding mechanism, binary LIF neurons ignore all membrane potentials with negative values, which may still carry valuable information. This limitation makes them less suitable for complex and high-dimensional tasks. To address this challenge, the ternary LIF neuron model was proposed [31, 32].

**Ternary LIF Neuron Model.** Spike encoding for the ternary LIF neuron is described by Equation (3). Both negative and positive membrane potentials are considered during encoding, which increases the representation capability of the neurons. Furthermore, since the ternary LIF encodes the membrane potential in values  $\{-1, 0, 1\}$ , it still preserves the multiplication-free property of the SNNs, which is critical in maintaining energy efficiency.

$$s^l(t) = \begin{cases} 1 & \text{if } m^l(t) \geq v^{\text{th}} \\ 0 & \text{if } -v^{\text{th}} < m^l(t) < v^{\text{th}} \\ -1 & \text{if } m^l(t) \leq -v^{\text{th}} \end{cases} \quad (3)$$

Although the ternary LIF improves the representation capacity of SNNs, experimental results for Q-learning tasks (see Table 4 in Section 5) show much lower performance compared to the binary LIF, which contradicts the results reported for other domains, such as language modeling and computer vision [31, 32]. This also challenges the mathematical analysis of Guo et al. on the increase in information entropy of the ternary LIF [31]. We would expect DSQN to perform better with increased representation capacity, whereas our observations indicate otherwise. This motivates us to develop a mathematical framework to resolve this contradiction and address both the performance degradation of ternary LIF neurons and the limited representation capacity of binary LIF neurons in Q-learning.

## 4 Methodology

First, we mathematically analyze spike encoding in SNNs and develop a hypothesis to explain the performance degradation observed when using ternary LIF neurons in DSQN. Building on the insights from this framework, we propose a novel ternary LIF model to overcome the limited representation capacity of the binary LIF. Finally, recognizing the importance of training stability in RL tasks, we mathematically prove that the proposed ternary LIF model ensures stable training dynamics by avoiding problems of gradient vanishing and exploding.

#### 4.1 Information Loss and Training Performance

We model the spikes as random variables by defining stochastic spikes [31, 32]. So, spikes are treated as random variables rather than having definite values, allowing us to describe their behavior in terms of the probability of taking on specific values and the probability distribution of the membrane potential, as defined by the following equations:

$$\tilde{s}^B = \begin{cases} 0 & p^0 = P(m(t) < v^{\text{th}}) \\ 1 & p^+ = P(m(t) \geq v^{\text{th}}) \end{cases} \quad (4)$$

$$\tilde{s}^T = \begin{cases} 1 & p^+ = P(m(t) \geq v^{\text{th}}) \\ 0 & p^0 = P(-v^{\text{th}} < m(t) < v^{\text{th}}) \\ -1 & p^- = P(m(t) \leq -v^{\text{th}}) \end{cases} \quad (5)$$

In the above,  $\tilde{s}^B$  and  $\tilde{s}^T$  denote stochastic binary and ternary spikes, respectively, and  $p^0$ ,  $p^+$ , and  $p^-$  are the probabilities of observing a zero spike, a positive spike, and a negative spike, respectively. We can define  $p^0$ ,  $p^+$ , and  $p^-$  based on the distance of  $m(t)$  to the thresholds and/or 0.

The probabilities defined above are determined by the distribution of the membrane potential,  $m(t)$ . Under certain conditions, which are mostly satisfied in general cases, we can show that the membrane potential  $m(t)$  of LIF neurons in the subthreshold regions tends to have a Gaussian-like distribution [54]. Consider an LIF neuron located in the first hidden layer of a large SNN. This neuron receives input in the form of spikes from the preceding (input) layer, each modulated by its corresponding synaptic weight. In the subthreshold regime, where the membrane potential remains below the firing threshold, the neuron's dynamics can be described by the continuous-time version of the LIF model (the continuous analog of Equation 2) as

$$\tau \frac{dm(t)}{dt} = -(m(t) - V_{\text{reset}}) + \sum_k \sum_{t_k^i} w_k \delta(t - t_k^i), \quad (6)$$

where  $\tau$  is the membrane time constant;  $w_k$  denotes the synaptic weight between the target neuron and the  $k$ -th input;  $t_k^i$  represents the time of the  $i$ -th spike from the  $k$ -th input;  $\delta(t)$  is the Dirac delta function; and  $m(t)$  and  $V_{\text{reset}}$  denote the membrane potential and the reset potential, respectively [54].

Assuming rate-based encoding in the input layer, where raw input values are converted into spike trains via Bernoulli sampling, and that the inputs are independent or only weakly correlated (a condition often satisfied in practice), the Central Limit Theorem implies that the aggregated input to a neuron can be approximated by a Gaussian distribution. To illustrate this in our setting, consider the first convolutional layer of a network, which uses an  $8 \times 8$  kernel and operates on inputs with four channels. We consider a flattened input of size 256, with each element independently drawn from a uniform distribution over  $[0, 1]$ , mimicking normalized raw pixel intensities. Each input element produces a spike with a probability proportional to its magnitude. For synaptic weights  $w_k$ , we use the kernel parameters of one of the best-performing models from our experiment section.

Figure 1 shows the resulting distribution of the term  $\sum_k \sum_{t_k^i} w_k \delta(t - t_k^i)$ , which represents the total weighted input current to a postsynaptic neuron. Thus, Equation 6 can be written as follows:

$$\tau \frac{dm(t)}{dt} = -(m(t) - V_{\text{reset}}) + \rho(t), \quad (7)$$

where  $\rho(t)$  is a white noise process representing the aggregated input  $\sum_k \sum_{t_k^i} w_k \delta(t - t_k^i)$ . We note that Equation 7 describes the Ornstein-Uhlenbeck stochastic process which satisfies the Fokker-Planck equation governing the evolution of the probability density function associated with the dynamics of the membrane potential [54]. This function is given by

$$\tau \frac{\partial}{\partial t} p(m, t) = -\frac{\partial}{\partial m} \left[ \left( -m + V_{\text{reset}} + \tau \sum_k w_k \nu_k(t) \right) p(m, t) \right] + \frac{1}{2} \xi^2 \frac{\partial^2}{\partial m^2} p(m, t), \quad (8)$$

where  $p(m, t)$  denotes the probability density of the neuron having membrane potential  $m$  at time  $t$ , and  $\nu_k(t)$  represents the spike rate of the  $k$ -th input. The term  $\xi$  is the time-dependent noise

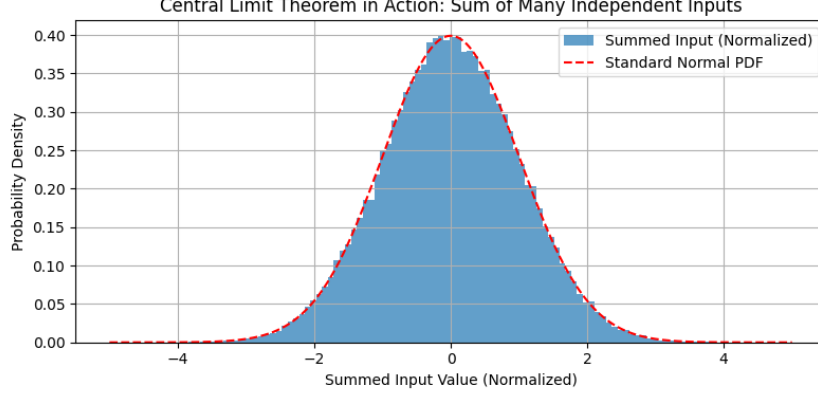


Figure 1: Approximate Gaussian distribution of the input term  $\sum_k \sum_{t_k^i} w_k \delta(t - t_k^i)$ , with 500 uniformly distributed inputs converted to spike trains via Bernoulli sampling.

amplitude, defined as follows:

$$\xi^2 = \tau \sum_k w_k \nu_k^2(t). \quad (9)$$

In the subthreshold regime, assuming  $\mathbb{E}[\rho(t)] \approx 0$ , which is convincing based on Figure 1, the expected trajectory of the membrane potential can be obtained by solving Equation 7, yielding the expression

$$m_0(t) = \mathbb{E}[m(t)] = V_{\text{reset}} \left(1 - e^{-t/\tau}\right). \quad (10)$$

Fluctuations in the membrane potential have a variance  $\sigma_m^2$ , which can be calculated as

$$\sigma_m^2(t) = \frac{1}{2} \xi^2 \left(1 - e^{-t/\tau}\right). \quad (11)$$

Finally, the solution to Equation 8 can be calculated as

$$p(m, t) = \frac{1}{\sqrt{2\pi\sigma_m^2(t)}} \exp\left(-\frac{(m(t) - m_0(t))^2}{2\sigma_m^2(t)}\right). \quad (12)$$

Equation 12 describes that  $p(m, t)$  follows a Gaussian-like distribution centered around  $m_0(t)$ . In most practical applications, it is common to assume  $V_{\text{reset}} = 0$ , in which case  $p(m, t)$  is centered around zero. Although Equation 12 describes the subthreshold behavior of an LIF neuron without a firing threshold, it can also be used to approximate the distribution of  $m(t)$  in LIF neurons with a spike-based threshold. In such cases, the spike threshold acts as an absorbing barrier: when the membrane potential reaches this threshold, it triggers a spike and resets, effectively truncating the upper tail of the distribution [54]. Combined with the reset mechanism, this causes the membrane potential to spend more time near  $V_{\text{reset}}$ , resulting in a distribution that is typically a truncated version of a Gaussian distribution.

The probabilities of observing a zero spike and a positive spike can be calculated for binary spiking neurons as

$$p^+ = \int_{v^{\text{th}}}^{\infty} p(m, t) dm, \quad p^0 = \int_{-\infty}^{v^{\text{th}}} p(m, t) dm \quad (13)$$

and for ternary spiking neurons that includes the negative spike as

$$p^+ = \int_{v^{\text{th}}}^{\infty} p(m, t) dm, \quad p^0 = \int_{-v^{\text{th}}}^{v^{\text{th}}} p(m, t) dm, \quad p^- = \int_{-\infty}^{-v^{\text{th}}} p(m, t) dm \quad (14)$$

For the binary case, we can write  $p^0 + p^+ = 1$ , and for the ternary case  $p^0 + p^- + p^+ = 1$ .

**Information Entropy Analysis.** Consider a set of random variables  $\mathcal{S}$ . The representation capability of  $\mathcal{S}$  can be quantified using its information entropy  $\mathcal{H}(\mathcal{S}) = -\sum_{s \in \mathcal{S}} P(s) \log P(s)$ , where  $P(s)$  is

Table 1: Commonly used surrogate gradient functions in SNNs

Name	Surrogate Function	Surrogate Gradient
<i>Atan</i>	$s^l(t) = \frac{1}{\pi} \arctan\left(\frac{\pi m(t)\alpha}{2}\right)$	$GE = \frac{\partial s^l(t)}{\partial m(t)} = \frac{1}{\pi} \cdot \frac{1}{1 + \left(\frac{\pi m(t)\alpha}{2}\right)^2}$
<i>STE</i>	$s^l(t) = m(t)$	$GE = \frac{\partial s^l(t)}{\partial m(t)} = 1$
<i>Sigmoid</i>	$s^l(t) = \frac{1}{1 + \exp(-km(t))}$	$GE = \frac{\partial s^l(t)}{\partial m(t)} = \frac{k \exp(-km(t))}{(\exp(-km(t)) + 1)^2}$

the probability of observing  $s \in \mathcal{S}$ .  $\mathcal{H}(\mathcal{S})$  reaches its maximum when all outcomes  $s \in \mathcal{S}$  are equally likely, that is,  $P(s)$  is uniform.

By assuming the same firing rate,  $r$ , we can use the concept of information entropy to compare the representation capacity of binary and ternary LIFs. For binary LIF, we have:  $\mathcal{S} = \{0, 1\}$ ,  $p^0 = 1 - r$ , and  $p^+ = r$ . For ternary LIF neurons, since the threshold  $v^{th}$  is symmetric for both the positive and negative domains, and the membrane potential  $m(t)$  follows a Gaussian-like distribution, the probabilities of generating positive and negative spikes are equal (see Equations 12 and 14). Thus, we have  $\mathcal{S} = \{-1, 0, 1\}$ ,  $p^0 = 1 - r$ , and  $p^- = p^+ = \frac{r}{2}$ . The information entropy of binary and ternary LIFs is calculated as

$$\mathcal{H}(\tilde{s}^B) = -r \ln r - (1 - r) \ln(1 - r) \text{ and } \mathcal{H}(\tilde{s}^T) = -r \ln\left(\frac{r}{2}\right) - (1 - r) \ln(1 - r) \quad (15)$$

As a result, we have  $\mathcal{H}(\tilde{s}^T) - \mathcal{H}(\tilde{s}^B) = r$ . Thus, ternary LIF increases the representation capacity of spiking neurons by at most  $r$  bits.

**Gradient Within the Network.** Although spike encoding is inherently non-differentiable due to the use of a threshold function (see Equation (3)), methods such as surrogate gradient learning (SGL) [29, 55, 56] and the straight-through estimator (STE) [33] offer effective solutions for training SNNs via backpropagation by estimating gradients. Some commonly used surrogate functions [57] are listed in Table 1. Here,  $\alpha$  and  $k$  are the model parameters, usually set to 2 and 25, respectively.

The expected value of the gradient estimators can be computed as

$$\mathbb{E}[GE(m, t)] = \int GE(m) p(m, t) dm. \quad (16)$$

Based on the commonly used pseudo-functions and the form of  $p(m, t)$  given in Equation 12, both  $GE(m)$  and  $p(m, t)$  are strictly positive for all  $m$ . Consequently, as shown in Equation 16, the expected value  $\mathbb{E}[GE(m, t)]$  is strictly greater than zero.

Taking into account the stochastic spike encoding introduced in Equation (4), we can calculate the expected value of the spike generation gradient needed for backpropagation through the SNN. This is given by

$$\mathbb{E}\left[\frac{\partial \tilde{s}^B}{\partial m(t)}\right] = \frac{\partial}{\partial m(t)} \mathbb{E}[\tilde{s}^B] = \frac{\partial}{\partial m(t)} (0 \cdot p^0 + 1 \cdot p^+) \quad (17)$$

$$\mathbb{E}\left[\frac{\partial \tilde{s}^T}{\partial m(t)}\right] = \frac{\partial}{\partial m(t)} \mathbb{E}[\tilde{s}^T] = \frac{\partial}{\partial m(t)} (0 \cdot p^0 - 1 \cdot p^- + 1 \cdot p^+) \quad (18)$$

For ternary LIF, where the probabilities are distributed among three possible outcomes, the maximum information entropy is achieved when  $p^- = p^+$ , reflecting a balanced and symmetric distribution. Also, recall from our previous discussion that the membrane potential of LIF neurons in the sub-threshold regime tends to follow a Gaussian-like distribution. From this result, we can make the following key observations related to the value of the expected gradient.

- For ternary neurons with symmetric thresholds, where  $v_p^{th} = v_n^{th}$ , we have  $p^+ = p^-$  (according to Equations 18 and 12). Thus, based on Equation 14, regardless of  $m(t)$ , the expected gradient becomes zero.
- For ternary neurons with asymmetric thresholds, where  $v_p^{th} \neq v_n^{th}$ , we have  $p^+ \neq p^-$  which results in a non-zero expected gradient.

- For *binary neurons*, using Equations 17, 12, and 13, the expected value of the gradient is also non-zero.

Since the expected value of the gradient is zero for the ternary LIF neuron with symmetric threshold, gradient estimators become biased, which reduces the accuracy of backpropagation. In contrast, binary-spiking neurons yield a non-zero expected gradient, resulting in a less biased gradient estimator (though still potentially biased). We hypothesize that this difference explains the observed performance degradation of SNNs using ternary LIF compared to those using binary LIF in Q-learning tasks. In RL tasks, the network’s gradient plays a vital role in shaping the trajectory of the dynamical system. The samples collected along these trajectories serve as training data. As the system approaches the optimal path, the training data become more informative and reliable. However, a greater bias in gradient estimation can drive the system toward inefficient paths, deteriorating the quality of the training data, and hindering the algorithm’s performance. In other machine learning tasks, such as computer vision and language modeling, the quality of the training data is independent of training performance, making these models more robust to biased gradient estimators. The findings of this mathematical analysis are summarized in the following Lemma.

**Lemma 4.1.** *Consider an SNN using the ternary LIF described in Equation (3). The network achieves maximum representation capacity when the expected value of the gradient through the network approaches zero.*

*Proof.* According to Equation (15), the maximum representation capacity of the ternary neuron is achieved when negative and positive spikes are equally likely, that is,  $p^+ = p^-$ . Then, according to Equation (18), the expected value of the gradient of the threshold function approaches zero. Thus, due to the chain rule in the backpropagation algorithm, the expected value of the gradient through the network also approaches zero.  $\square$

*Remark 4.2.* Since the expected values of the gradient estimators are nonzero, the use of ternary LIF introduces a high bias in the gradient estimation, resulting in overestimation or underestimation of the gradients. This bias adversely affects the network’s training performance.

## 4.2 Asymmetric Ternary LIF Neuron

Based on the insight provided by Lemma 4.1 and Remark 4.2, and our hypothesis, although our goal is to enhance the representation capacity of SNNs, we aim to avoid reaching maximum information entropy, as this makes the gradient estimators more biased during backpropagation. Given that the membrane potential of LIF neurons tends to follow a Gaussian-like distribution in the subthreshold region, if the firing thresholds for positive and negative spikes are symmetric, as is the case in existing ternary LIF models, it is likely that  $p^+ = p^-$ . This symmetry in spiking behavior causes the expected value of the gradient to become zero, which, as discussed in Section 4.1, leads to a more biased gradient estimation. To overcome this issue while still benefiting from the increased representation capacity of ternary neurons, we propose an asymmetric ternary spiking model, as follows:

$$s^l(t) = \begin{cases} 1 & \text{if } m^l(t) \geq v^{\text{th}_p} \\ 0 & \text{if } -v^{\text{th}_n} < m^l(t) < v^{\text{th}_p} \\ -1 & \text{if } m^l(t) \leq -v^{\text{th}_n} \end{cases} \quad (19)$$

where  $v^{\text{th}_p}$  and  $v^{\text{th}_n}$  are the positive and negative firing thresholds, respectively, and  $v^{\text{th}_p} \neq v^{\text{th}_n}$ .

Given that the representation capacity and training performance of the network are two competing factors and based on the Gaussian-like distribution of the membrane potential, are a function of  $v^{\text{th}_p}$  and  $v^{\text{th}_n}$ , we propose fixing  $v^{\text{th}_p}$  at a constant value and treating  $v^{\text{th}_n}$  as a trainable parameter. This approach enables the optimizer to adjust  $v^{\text{th}_n}$  together with other trainable parameters, allowing the network to implicitly influence the bias of the chosen gradient estimator. We now show that the proposed asymmetric ternary model enhances the information entropy and prevents the expected value of the gradient from becoming zero.

**Theorem 4.3.** *For binary and asymmetric ternary spiking neuron models described in Equations (2) and (19), respectively, and for the same firing rate  $r$ , the asymmetric ternary model achieves higher representation capacity and ensures that the expected value of its gradient remains nonzero.*

*Proof.* The representation capacity can be quantified by the information entropy. For binary LIF,  $S = \{0, 1\}$ ,  $p^0 = 1 - r$ , and  $p^+ = r$ . For asymmetric ternary LIF, given that  $v^{\text{th}_n} \neq v^{\text{th}_p}$  in general,

we can write:  $\mathcal{S} = \{-1, 0, 1\}$ ,  $p^0 = 1 - r$ ,  $p^- + p^+ = r$ . Assume that  $p^- = r_1$  and  $p^+ = r_2$ . We can calculate the information capacity of the binary LIF and the asymmetric ternary LIF as

$$\mathcal{H}(\tilde{s}^B) = -r \ln r - (1 - r) \ln(1 - r) \text{ and } \mathcal{H}(\tilde{s}^{AT}) = -r_1 \ln r_1 - r_2 \ln r_2 - (1 - r) \ln(1 - r)$$

Since  $r = r_1 + r_2$ ,  $\mathcal{H}(\tilde{s}^{AT}) - \mathcal{H}(\tilde{s}^B) = -r_1 \ln\left(\frac{r_1}{r}\right) - r_2 \ln\left(\frac{r_2}{r}\right)$  and since  $r_1, r_2 > 0$ , we can conclude that  $-r_1 \ln\left(\frac{r_1}{r}\right) - r_2 \ln\left(\frac{r_2}{r}\right) > 0$ , which means an increase in the information entropy, leading to higher representation capability of the asymmetric ternary LIF compared to the binary LIF. The expected value of the gradient for the asymmetric ternary LIF can be calculated in the same manner as described by Equation(18). In this case, because  $p^- \neq p^+$ , the expected value of the gradient is nonzero, and the proof is completed.  $\square$

### 4.3 Analysis of Training Stability

Given the importance of training dynamics in RL tasks, we analyze the training behavior of SNNs employing asymmetric ternary spiking neurons through the lens of block dynamical isometry [32, 33], focusing on their susceptibility to the exploding or vanishing gradient problem. Consider a neural network as a series of blocks  $f(x) = f_{\theta^L}^L \circ f_{\theta^{L-1}}^{L-1} \cdots \circ f_{\theta^1}^1(x)$ , where  $f_{\theta^j}^j$  represents the  $j$ -th layer of the network, and  $\theta^j$  denotes the trainable parameters of layer  $j$ . The Jacobian matrix for block  $j$  is defined as  $J_j = \frac{\partial f^j}{\partial f^{j-1}}$ . If we define  $\phi(J) = \mathbb{E}[\text{tr}(J)]$ , then  $\varphi(J) = \phi(J^2) - \phi(J)^2$ .

**Definition 4.4.** Consider a neural network that can be represented as a sequence of blocks.  $J_j$  denotes the  $j$ -th block's Jacobian matrix. If  $\forall j, \phi(J_j J_j^T) \approx 1$ , and  $\varphi(J_j J_j^T) \approx 0$ , then the network achieves block dynamical isometry [33].

A network that achieves dynamical isometry avoids vanishing or exploding gradients during training by maintaining all values of its input-output Jacobian matrix  $\approx 1$ . We analyze the dynamical isometry of networks composed of asymmetric spiking neurons. Given the widespread success of the ReLU activation function in enabling stable training across various machine learning tasks, we compare the block isometry of networks using asymmetric ternary neurons to those employing ReLU activations.

**Lemma 4.5.** *If the probability of the input being greater than 0 is  $p$  and the network uses ReLU functions, then  $\phi(J_j J_j^T) = p$  and  $\varphi(J_j J_j^T) = p - p^2$  [33].*

**Lemma 4.6.** *If the spike firing rate of neurons is  $r$ , and the network uses asymmetric ternary spiking neurons as described in Equation (19), then  $\phi(J_j J_j^T) = 1 - r$  and  $\varphi(J_j J_j^T) = r - r^2$ .*

*Proof.* In networks with asymmetric ternary spiking neurons, the key factor in computing the Jacobian is the gradient of the threshold function defined in Equation (19). We denote its Jacobian as  $s_m$ , which forms a diagonal matrix due to the element-wise nature of the function. During backpropagation, gradient estimators such as STE are applied. Given the reset mechanism in Equation (2), the membrane potential  $m(t)$  remains within  $(-v^{th_n}, v^{th_p})$ , so the entries of  $s_m$  are 1 when  $m(t) \in (-v^{th_n}, v^{th_p})$ , and 0 otherwise. Thus, the probability density function of  $s_m$  can be defined as:  $\rho_{s_m}(z) = r\delta(z) + (1 - r)\delta(z - 1)$ . Since the values of  $s_m$  matrix are binary, it follows that  $\rho_{s_m s_m^T}(z) = \rho_{s_m}(z)$ . Thus,

$$\begin{aligned} \phi(s_m s_m^T) &= \int z \rho_{s_m s_m^T}(z) dz = 1 - r \\ \varphi(s_m s_m^T) &= \int z^2 \rho_{s_m s_m^T}(z) dz - \left( \int z \rho_{s_m s_m^T}(z) dz \right)^2 = r - r^2 \end{aligned} \tag{20}$$

$\square$

**Theorem 4.7.** *The asymmetric ternary spiking neuron achieves at least the dynamical isometry of ReLU activations, that is,  $\phi(s_m s_m^T) \geq \phi(J_j J_j^T)$  and  $\varphi(s_m s_m^T) \leq \varphi(J_j J_j^T)$ .*

*Proof.* The value of  $p$  for the zero-mean input distribution is around 0.5, while the firing rate in SNNs is usually between 0.1 and 0.5. Thus, based on Lemmas 4.5 and 4.6, we conclude that  $\phi(s_m s_m^T) \geq \phi(J_j J_j^T)$  and  $\varphi(s_m s_m^T) \leq \varphi(J_j J_j^T)$ .  $\square$

Table 2: Parameters of the convolution layers. Table 3: Parameters of the spiking neuron model.

Layers	Num. kernels	Kernel size	Stride	Parameter	Value
conv1	32	$8 \times 8$	4	Simulation time window ( $\mathcal{T}$ )	20
conv2	64	$4 \times 4$	2	Decay factor ( $\beta$ )	0.9
conv3	64	$3 \times 3$	1	Firing threshold ( $v^{th}$ or $v^{th_p}$ )	1
				Reset potential ( $v_{reset}$ )	0
				Learning rate	0.00005

Theorem 4.7 ensures the training stability of SNNs using our proposed neuron in various machine learning applications.

**Biological Persuasion.** Biology classifies neurons as excitatory or inhibitory, with approximately four out of every five neurons being excitatory. Research indicates that when 75–81% neurons are excitatory, the brain’s ability to solve complex problems is maximized [58, 59]. The ternary spiking neuron model allows neurons to exhibit both excitatory (emitting +1) and inhibitory (emitting -1) behaviors. The basic ternary LIF model described in Equation (3) makes the neuron respond symmetrically: its inhibitory effect for negative inputs mirrors its excitatory effect for positive inputs. However, this symmetry contradicts biological evidence. In contrast, the asymmetric ternary spiking neuron model described in Equation (19) introduces a remedy to this issue: it enables neurons to exhibit a dominance of excitatory or inhibitory behavior, aligning more closely with the brain’s mechanisms for solving complex tasks.

## 5 Experiments

We first examine our hypothesis that gradient estimation bias is a key factor contributing to the observed performance degradation of ternary LIF neurons. We then evaluate the impact of increasing the representation capacity, provided by our proposed asymmetric ternary neuron, which is motivated by this hypothesis, on the performance of SNNs in Q-learning tasks.

**Experimental Setup.** Seven games from the OpenAI Gym Atari environment [60] were arbitrarily selected for our evaluation. Liu et al. demonstrated that SNNs using binary spiking neurons can achieve human-level performance on Atari tasks [29]. However, their approach relies on a simulation time window of 40, leading to high decision-making latency. To make the task more challenging while reducing latency, our experiments use a shorter simulation time window of 20. When discussing the results, we refer to binary spiking neuron-based DQN, ternary spiking neuron-based DQN, and asymmetric ternary spiking neuron-based DQN as DSQN, DTSQL, and DATSQL, respectively.

**Network Architecture.** We adopt the architecture used in [29], and originally proposed by [36]. It consists of three convolutional layers followed by two fully connected layers. The first fully connected layer contains 512 neurons, while the second layer has between 4 and 18 neurons, depending on the number of possible actions in each game. All neurons in the network are spiking neurons of the same type: binary, ternary, or asymmetric ternary, depending on the selected neuron model.

Details pertaining to network architecture and hyperparameters are provided in Tables 2 and 3. The hyperparameters of the spiking neurons were selected as follows: We set the positive threshold voltage to  $v^{th_p} = v^{th} = 1$  based on the work reported in [31, 51], which reported empirical performance gains using this setting. For DATSQL, the negative threshold  $v^{th_n}$  was initialized to 2 and implemented as a learnable parameter using `nn.Parameter()`, allowing it to be updated through standard gradient-based optimization along with other network weights. The optimal values for the decay factor  $\beta$  and the learning rate were selected by trial and error using the Breakout game, as these parameters significantly affect both the training dynamics and the final performance. The process of forward propagation through the network is presented in Algorithm 1.

**Input Encoding.** In [29], raw pixel values are directly used as input to the SNN, requiring floating-point multiplications in the first layer and resulting in a non-spiking first layer. To enable a fully spiking network, consistent with the principles of neuromorphic hardware, we apply rate-based encoding to convert raw pixel values into spike trains. This ensures compatibility with spike-based computation and reduces the dependence on costly floating-point operations.

We first normalize the input pixel values in the range  $[0, 1]$  by dividing them by 255. The spikes were then generated using Bernoulli sampling, where the probability of firing was proportional to the normalized pixel intensity. We also experimented with the rate encoding module from the

---

**Algorithm 1** Forward propagation through DSQN-DTSQN-DATSQN

---

- 1: Randomly initialize weight and kernel matrices  $\mathbf{W}$  and biases  $\mathbf{b}$  for each SNN layer;
  - 2: Initialize membrane potentials,  $v^k(0)$  by 0;
  - 3:  $(M \times N \times N)$ -dimensional observation state,  $I$ ;
  - 4: Spikes from input generated by the rate encoder module:  $\mathbf{X} = \text{Encoder}(\mathbf{I})$ ;
  - 5: **for**  $t = 1, \dots, T$  **do**
  - 6:   Spikes from input encoder at timestep  $t$ :  $s^0(t) = \mathbf{X}(t)$
  - 7:   **for**  $k = 1, \dots, K - 1$  **do**
  - 8:     Update LIF neurons in layer  $k$  at timestep  $t$  based on spikes from layer  $k - 1$ :
  - 9:      $m^k(t) = v^k(t - 1) + \mathbf{W}^k s^{k-1}(t) + \mathbf{b}^k$
  - 10:      $s^k(t) = \text{Threshold}(m^k(t))$
  - 11:      $v^k(t) = \beta m^k(t)(1 - s^k(t)) + v_{\text{reset}} s^k(t)$
  - 12: Sum up the spikes of output layer:  $\mathbf{Q} = \sum_{t=1}^T \mathbf{W}^K s^{K-1}(t) + \mathbf{b}^K$
- 

Table 4: Scores achieved by DSQN, DTSQN, and DATSQN.

Game	DSQN score $\pm$ (std)	DTSQN score $\pm$ (std)	DATSQN score $\pm$ (std)
Beam Rider	2069 $\pm$ (580.4)	1518.6 $\pm$ (529.7)	<b>4000 <math>\pm</math> (967.25)</b>
Boxing	79.3 $\pm$ (9.5)	49.1 $\pm$ (18.5)	79.1 $\pm$ (7.1)
Breakout	207.7 $\pm$ (64)	23.6 $\pm$ (6.5)	<b>252.14 <math>\pm</math> (70)</b>
Crazy Climber	53230 $\pm$ (11660)	4240 $\pm$ (1110)	<b>54190 <math>\pm</math> (13921)</b>
Gopher	1842 $\pm$ (465)	1162 $\pm$ (564.06)	<b>2111.1 <math>\pm</math> (648)</b>
Jamesbond	185 $\pm$ (109)	120 $\pm$ (52)	<b>250 <math>\pm</math> (140)</b>
SpaceInvaders	457 $\pm$ (64.8)	324 $\pm$ (102.3)	<b>655 <math>\pm</math> (123.7)</b>

Table 5: Performance difference between DTSQN &amp; DATSQN.

Game	DTSQN score (%)	DATSQN score (%)
Beam Rider	73%	193%
Boxing	62%	100%
Breakout	11%	121%
Crazy Climber	8%	102%
Gopher	63%	114%
Jamesbond	65%	135%
Space Invaders	71%	143%
Average (%) w.r.t. DSQN	50%	130%

*snnTorch* [57] library, which generates spikes based on a Poisson distribution. The results remained largely consistent across both methods. This input encoding approach was applied uniformly across all model variants: DSQN, DTSQN, and DATSQN. The input spikes propagate through the network, and at each time step, the LIF neurons preceding the output layer emit 0 or +1 in DSQN, and 0, +1, or -1 in DTSQN and DATSQN. These spikes are passed through a linear layer to produce intermediate outputs. The final network outputs are obtained by summing these intermediate outputs over the entire simulation time window. Algorithm 1 describes the forward inference pass through the SNN for a simulation window of  $T$  time steps.

**Testing and Metrics.** We train SNNs with an  $\epsilon$ -greedy algorithm ( $\epsilon = 0.1$ ) over  $10^6$  steps. For each agent, we select the model that achieves the highest reward during training and report its average score and standard deviation over 10 evaluation episodes. To facilitate comparison, we also normalize the DTSQN and DATSQN scores with respect to the DSQN score.

**Performance Analysis.** Table 4 reports the scores for three RL agents in seven games. DATSQN consistently achieves higher scores than DSQN, while DTSQN shows a clear performance drop in every game. These results support our hypothesis because the asymmetric design addresses the performance issues of ternary neurons in Q-learning. The improvement achieved by DATSQN over DSQN is likely due to the increased representation capacity of ternary neurons. We also note that the DSQN scores are lower than those reported in [29], which can be attributed to two main differences.

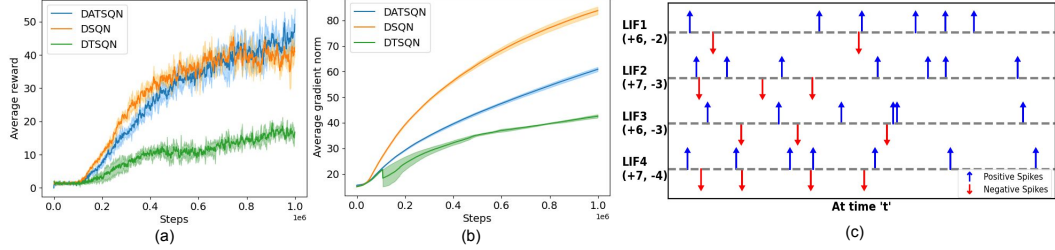


Figure 2: (a) Learning curves, (b) average gradient norm across the network during training for each RL agent, and (c) excitatory and inhibitory spikes generated by randomly selected neurons in the breakout environment.

First, their first layer is non-spiking, which relies on floating-point computation and is less compatible with neuromorphic hardware. Second, we use a shorter simulation time window to reduce latency, making tasks more challenging.

To highlight the performance gains of the proposed asymmetric ternary neuron model, Table 5 shows a comparative analysis between DTSQN and DATSQN where the scores are normalized with respect to the baseline (the binary neuron-based DSQN).

**Training Dynamics.** Figure 2 shows the average cumulative reward during training and the average gradient norm for the three agents in the Breakout environment. As Fig. 2 (a) indicates, DTSQN consistently shows a degraded performance compared to the state-of-the-art DSQN. Furthermore, based on Fig. 2 (b), DTSQN has the lowest average gradient norm among all three agents, (in line with Lemma 4.1). During the initial training steps, DSQN shows better performance than DATSQN in terms of the cumulative reward achieved. However, during the final stages of training, DATSQN achieves a higher cumulative reward (sign of increased representation capacity). It is important to note that when the reward is high, typically in the final stage of the game and near human-level performance, even a small improvement in reward can lead to a substantial increase in the overall game score and potentially alter the outcome entirely. The average gradient norm during training remains stable, showing no sudden spikes or sharp drops, indicating no signs of vanishing or exploding gradients.

To better understand learning behavior, we randomly select some neurons with asymmetric domains from each layer of various SNN models. We then examine neurons within a randomly chosen feature map from a subsequent convolutional layer, tracking the number of positive and negative spikes originating from the  $(k_h \times k_w)$  region of the previous layer’s feature map that contributed to each neuron in that layer. This process closely resembles convolution, where a region of interest interacts with a kernel of size  $(k_h \times k_w)$ . We analyze how many positive and negative spikes from this region participate in the convolution process. Empirical observations in all models and layers consistently show that the number of positive spikes exceeds the number of negative spikes, with the ratio  $\geq 65\%$ . Figure 2 (c) illustrates this phenomenon using four neurons from a feature map in the second convolutional layer, tracking the positive and negative spikes that arrive from a  $(4 \times 4)$  region of the feature map of the previous layer.

Positive spikes act as excitatory impulses, whereas negative spikes are inhibitory. Our SNN model that uses ternary neurons with an asymmetric domain effectively mimics a fundamental property of the human brain, where approximately 70–80% of neurons are excitatory, and the remainder are inhibitory [58, 59]. Studies suggest that this imbalance between excitatory and inhibitory neurons is crucial for efficient information processing, learning, and overall neural computation. For DRL tasks that require adaptive decision making in dynamic environments, we believe that LIF neurons with asymmetric domains can play a critical role in facilitating effective learning by maintaining an optimal excitation-inhibition balance.

**Ablation Study.** We attributed the improved performance of DATSQN to enhanced gradient estimation quality, which prevents the expected value of the gradient from decreasing toward zero. However, this improvement may also come from the inclusion of a trainable threshold in the ternary neuron model. To investigate this further, we conduct an ablation study by training DTSQN with the trainable threshold, that is, making  $v^{\text{th}}$  in Equation 3 a trainable parameter. The results, shown in Figure 3 (a), indicate that introducing a trainable threshold only marginally improves the performance of DTSQN.

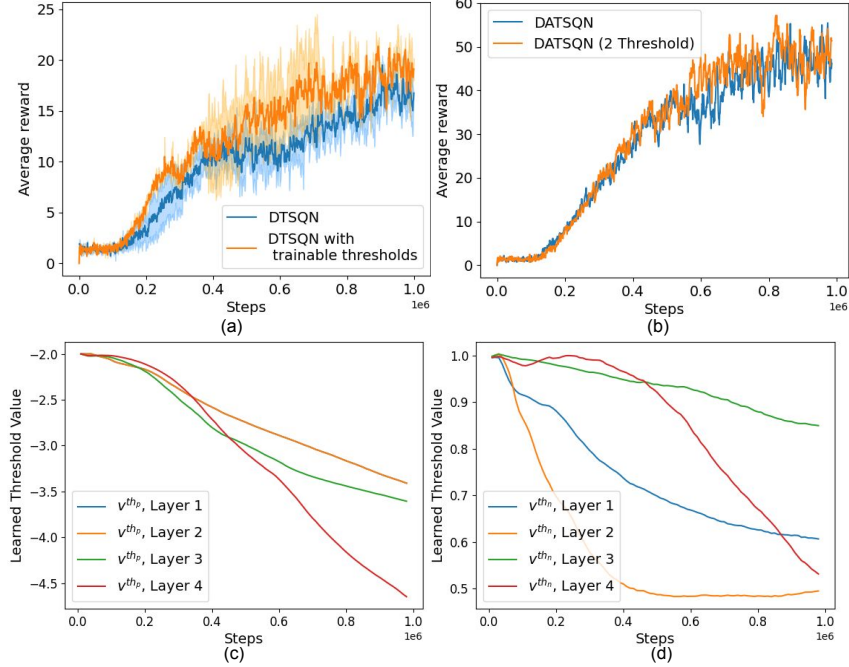


Figure 3: Learning curves for (a) DSQN with and without trainable thresholds, and (b) DATSQN with one versus two trainable threshold parameters in the Breakout environment. Dynamic evolution of the negative thresholds (c) and the positive thresholds (d) in asymmetric ternary spiking neurons within the hidden layers of DATSQN.

Despite improvements, a substantial performance gap remains relative to baseline (DSQN). A likely explanation is that with only one threshold parameter, the positive and negative thresholds remain symmetric, and as shown in Lemma 4.1, the expected gradient still tends to zero.

Our final set of experiments uses DATSQN, where neurons are equipped with two independent trainable thresholds. The results, shown in Fig. 3 (b), indicate that this modification does not greatly improve performance. The dynamic evolution of these thresholds during training is shown in Fig. 3 (c) and (d), where the network decreases the absolute value of the positive threshold while increasing that of the negative threshold. Since the network is optimized to maximize cumulative rewards, this behavior suggests that neurons tend to act more excitatory than inhibitory, supporting the biologically inspired motivation discussed in Section 4.

## 6 Discussion

This paper investigates the use of ternary spiking neurons to improve the performance of SNNs in Q-learning tasks by increasing their representation capacity. Motivated by both mathematical analysis and biological insights, we propose a new ternary spiking neuron model called the asymmetric ternary spiking neuron to address the performance degradation seen in state-of-the-art ternary models, and we provide a potential mathematical explanation for the observed performance degradation. Our results show that the proposed model achieves much better performance compared to binary SNNs in Q-learning tasks.

Although demonstrated in the context of Q-learning, the proposed model and framework are broadly applicable and hold promise for a wide range of machine learning domains, including computer vision, natural language processing, and control systems. By improving the representation capacity of SNNs, which is a widely recognized challenge for developing applications of neuromorphic computing, this research contributes to closing the gap between energy-efficient neuromorphic systems and traditional deep learning models. These advances may accelerate the deployment of SNN-based solutions in low-power settings such as edge computing, autonomous robotics, and embedded AI. Moreover, the theoretical insights provided here may inform future innovations in neuromorphic computing and spur research at the intersection of neuroscience, machine learning, and hardware design.

## References

- [1] Yuke Zhu, Roozbeh Mottaghi, Eric Kolve, Joseph J Lim, Abhinav Gupta, Li Fei-Fei, and Ali Farhadi. Target-driven visual navigation in indoor scenes using deep reinforcement learning. In *2017 IEEE international conference on robotics and automation (ICRA)*, pages 3357–3364. IEEE, 2017.
- [2] Sehoon Ha, Joohyung Kim, and Katsu Yamane. Automated deep reinforcement learning environment for hardware of a modular legged robot. In *2018 15th international conference on ubiquitous robots (UR)*, pages 348–354. IEEE, 2018.
- [3] Han Hu, Kaicheng Zhang, Aaron Hao Tan, Michael Ruan, Christopher Agia, and Goldie Nejat. A sim-to-real pipeline for deep reinforcement learning for autonomous robot navigation in cluttered rough terrain. *IEEE Robotics and Automation Letters*, 6(4):6569–6576, 2021.
- [4] Shuwei Zhang, Yutian Wu, Harutoshi Ogai, Hiroshi Inujima, and Shigeyuki Tateno. Tactical decision-making for autonomous driving using dueling double deep q network with double attention. *IEEE Access*, 9:151983–151992, 2021.
- [5] JiaKui Hu, Man Yao, Xuerui Qiu, Yuhong Chou, Yuxuan Cai, Ning Qiao, Yonghong Tian, XU Bo, and Guoqi Li. High-performance temporal reversible spiking neural networks with  $o(l)$  training memory and  $o(1)$  inference cost. In *Forty-first International Conference on Machine Learning*, 2024.
- [6] Samanwoy Ghosh-Dastidar et al. Spiking neural networks. *J. Neural Systems*, pages 295–308, 2009.
- [7] E. M. Izhikevich. Simple model of spiking neurons. *IEEE Trans. Neural Net.*, 14(6):1569–1572, Nov 2003.
- [8] Yongqiang Cao, Yang Chen, and Deepak Khosla. Spiking deep convolutional neural networks for energy-efficient object recognition. *Int’l J. Computer Vision*, 113:54–66, 2015.
- [9] Yujie Wu, Lei Deng, Guoqi Li, and Luping Shi. Spatio-temporal backpropagation for training high-performance spiking neural networks. *Frontiers in neuroscience*, 12:323875, 2018.
- [10] Chankyu Lee, Syed Shakib Sarwar, Priyadarshini Panda, Gopalakrishnan Srinivasan, and Kaushik Roy. Enabling spike-based backpropagation for training deep neural network architectures. *Frontiers in neuroscience*, 14:497482, 2020.
- [11] Changze Lv, Jianhan Xu, and Xiaoqing Zheng. Spiking convolutional neural networks for text classification. In *Int’l Conf. Learning Representations (ICLR)*, 2022.
- [12] Francisco Naveros, Niceto R Luque, Jesús A Garrido, Richard R Carrillo, Mancía Anguita, and Eduardo Ros. A spiking neural simulator integrating event-driven and time-driven computation schemes using parallel cpu-gpu co-processing: a case study. *IEEE transactions on neural networks and learning systems*, 26(7):1567–1574, 2014.
- [13] Corinne Teeter, Ramakrishnan Iyer, Vilas Menon, Nathan Gouwens, David Feng, Jim Berg, Aaron Szafer, Nicholas Cain, Hongkui Zeng, Michael Hawrylycz, et al. Generalized leaky integrate-and-fire models classify multiple neuron types. *Nature communications*, 9(1):709, 2018.
- [14] Catherine D Schuman, Shruti R Kulkarni, Maryam Parsa, J Parker Mitchell, Prasanna Date, and Bill Kay. Opportunities for neuromorphic computing algorithms and applications. *Nature Computational Science*, 2(1):10–19, 2022.
- [15] S. Moradi, N. Qiao, F. Stefanini, and G. Indiveri. A scalable multicore architecture with heterogeneous memory structures for dynamic neuromorphic asynchronous processors (DYNAPs). *Biomedical Circuits and Systems, IEEE Transactions on*, 12(1):106–122, Feb. 2018.
- [16] Mike Davies, Narayan Srinivasa, Tsung-Han Lin, Gautham Chinya, Yongqiang Cao, Sri Harsha Choday, Georgios Dimou, Prasad Joshi, Nabil Imam, Shweta Jain, et al. Loihi: A neuromorphic manycore processor with on-chip learning. *Ieee Micro*, 38(1):82–99, 2018.

- [17] Brien M. Posey. Akida event domain neural processor. Technical report, Brainchip, 2023.
- [18] Michael V. Debole, Brian Taba, Arnon Amir, et al. TrueNorth: Accelerating from zero to 64 million neurons in 10 years. *Computer*, 2019.
- [19] Ahmed M Abdelsalam, Felix Boulet, et al. An efficient FPGA-based overlay inference architecture for fully connected DNNs. In *Proc. IEEE Conf. Reconfigurable Computing & FPGAs (ReConFig)*, pages 1–6, 2018.
- [20] Federico Corradi, Guido Adriaans, and Sander Stuijk. Gyro: A digital spiking neural network architecture for multi-sensory data analytics. In *Proc. ACM Drone Syst. Eng. & Rapid Simulation & Perf. Eval.*, page 9–15, 2021.
- [21] Sixu Li, Zhaomin Zhang, Ruixin Mao, Jianbiao Xiao, Liang Chang, and Jun Zhou. A fast and energy-efficient SNN processor with adaptive clock/event-driven computation scheme and online learning. *IEEE Trans. Circuits & Systems I*, 68(4):1543–1552, 2021.
- [22] Hanwen Liu, Yi Chen, Zihang Zeng, Malu Zhang, et al. A low power and low latency FPGA-based spiking neural network accelerator. In *IEEE Int’l Joint Conf. Neural Networks (IJCNN)*, pages 1–8, 2023.
- [23] Alessio Carpegna, Alessandro Savino, and Stefano Di Carlo. Spiker: An FPGA-optimized hardware accelerator for spiking neural networks. In *IEEE Computer Society Annual Symp. VLSI (ISVLSI)*, pages 14–19, 2022.
- [24] Shadi Matiniazadeh et al. A fully-configurable open-source software-defined digital quantized spiking neural core architecture. In *IEEE Int’l Midwest Symp. Circuits & Systems (MWSCAS)*, 2024.
- [25] Shuo Feng, Jian Cao, Zehong Ou, Guang Chen, Yi Zhong, Zilin Wang, Juntong Yan, Jue Chen, Bingsen Wang, Chenglong Zou, et al. Brainqn: Enhancing the robustness of deep reinforcement learning with spiking neural networks. *Advanced Intelligent Systems*, 6(9):2400075, 2024.
- [26] Guangzhi Tang, Neelesh Kumar, Raymond Yoo, and Konstantinos Michmizos. Deep reinforcement learning with population-coded spiking neural network for continuous control. In *Conference on Robot Learning*, pages 2016–2029. PMLR, 2021.
- [27] Nitin Rathi, Gopalakrishnan Srinivasan, Priyadarshini Panda, and Kaushik Roy. Enabling deep spiking neural networks with hybrid conversion and spike timing dependent backpropagation. *arXiv preprint arXiv:2005.01807*, 2020.
- [28] Devdhar Patel, Hananel Hazan, Daniel J Saunders, Hava T Siegelmann, and Robert Kozma. Improved robustness of reinforcement learning policies upon conversion to spiking neuronal network platforms applied to atari breakout game. *Neural Networks*, 120:108–115, 2019.
- [29] Guisong Liu, Wenjie Deng, Xiurui Xie, Li Huang, and Huajin Tang. Human-level control through directly trained deep spiking q-networks. *IEEE transactions on cybernetics*, 53(11): 7187–7198, 2022.
- [30] Guangzhi Tang, Neelesh Kumar, and Konstantinos P Michmizos. Reinforcement co-learning of deep and spiking neural networks for energy-efficient mapless navigation with neuromorphic hardware. In *2020 IEEE/RSJ International Conference on Intelligent Robots and Systems (IROS)*, pages 6090–6097. IEEE, 2020.
- [31] Yufei Guo, Yuanpei Chen, Xiaode Liu, Weihang Peng, Yuhan Zhang, Xuhui Huang, and Zhe Ma. Ternary spike: Learning ternary spikes for spiking neural networks. In *Proceedings of the AAAI Conference on Artificial Intelligence*, volume 38, pages 12244–12252, 2024.
- [32] Xingrun Xing, Zheng Zhang, Ziyi Ni, Shitao Xiao, Yiming Ju, Siqi Fan, Yequan Wang, Jiajun Zhang, and Guoqi Li. Spikelm: Towards general spike-driven language modeling via elastic bi-spiking mechanisms. *arXiv preprint arXiv:2406.03287*, 2024.
- [33] Zhaodong Chen, Lei Deng, Bangyan Wang, Guoqi Li, and Yuan Xie. A comprehensive and modularized statistical framework for gradient norm equality in deep neural networks. *IEEE Transactions on Pattern Analysis and Machine Intelligence*, 44(1):13–31, 2020.

- [34] Shengbo Eben Li. *Reinforcement learning for sequential decision and optimal control*. Springer, 2023.
- [35] Volodymyr Mnih. Playing atari with deep reinforcement learning. *arXiv preprint arXiv:1312.5602*, 2013.
- [36] Volodymyr Mnih, Koray Kavukcuoglu, David Silver, Andrei A Rusu, Joel Veness, Marc G Bellemare, Alex Graves, Martin Riedmiller, Andreas K Fidjeland, Georg Ostrovski, et al. Human-level control through deep reinforcement learning. *nature*, 518(7540):529–533, 2015.
- [37] Hado Van Hasselt, Arthur Guez, and David Silver. Deep reinforcement learning with double q-learning. In *Proceedings of the AAAI conference on artificial intelligence*, volume 30, 2016.
- [38] Ziyu Wang, Tom Schaul, Matteo Hessel, Hado Hasselt, Marc Lanctot, and Nando Freitas. Dueling network architectures for deep reinforcement learning. In *International conference on machine learning*, pages 1995–2003. PMLR, 2016.
- [39] Mohit Sewak and Mohit Sewak. Deep q network (dqn), double dqn, and dueling dqn: A step towards general artificial intelligence. *Deep reinforcement learning: frontiers of artificial intelligence*, pages 95–108, 2019.
- [40] Weihao Tan, Devdhar Patel, and Robert Kozma. Strategy and benchmark for converting deep q-networks to event-driven spiking neural networks. In *Proceedings of the AAAI conference on artificial intelligence*, volume 35, pages 9816–9824, 2021.
- [41] Yinqian Sun, Yi Zeng, and Yang Li. Solving the spike feature information vanishing problem in spiking deep q network with potential based normalization. *Frontiers in Neuroscience*, 16: 953368, 2022.
- [42] Mahmoud Akl, Deniz Ergene, Florian Walter, and Alois Knoll. Toward robust and scalable deep spiking reinforcement learning. *Frontiers in Neurobotics*, 16:1075647, 2023.
- [43] Shuai Zhang, Heshan Devaka Fernando, Miao Liu, Keerthiram Murugesan, Songtao Lu, Pin-Yu Chen, Tianyi Chen, and Meng Wang. SF-dqn: Provable knowledge transfer using successor feature for deep reinforcement learning. *arXiv preprint arXiv:2405.15920*, 2024.
- [44] Liangheng Lv, Sunjie Zhang, Derui Ding, and Yongxiong Wang. Path planning via an improved dqn-based learning policy. *IEEE Access*, 7:67319–67330, 2019.
- [45] Todd Hester, Matej Vecerik, Olivier Pietquin, Marc Lanctot, Tom Schaul, Bilal Piot, Dan Horgan, John Quan, Andrew Sendonaris, Ian Osband, et al. Deep q-learning from demonstrations. In *Proceedings of the AAAI conference on artificial intelligence*, volume 32, 2018.
- [46] Jingwei Lu, Liyuan Han, Qinglai Wei, Xiao Wang, Xingyuan Dai, and Fei-Yue Wang. Event-triggered deep reinforcement learning using parallel control: A case study in autonomous driving. *IEEE Transactions on Intelligent Vehicles*, 8(4):2821–2831, 2023.
- [47] Dan Horgan, John Quan, David Budden, Gabriel Barth-Maron, Matteo Hessel, Hado Van Hasselt, and David Silver. Distributed prioritized experience replay. *arXiv preprint arXiv:1803.00933*, 2018.
- [48] RB Stein and Alan Lloyd Hodgkin. The frequency of nerve action potentials generated by applied currents. *Proceedings of the Royal Society of London. Series B. Biological Sciences*, 167(1006):64–86, 1967.
- [49] Zhengyang Zhuge, Peisong Wang, Xingting Yao, and Jian Cheng. Towards efficient spiking transformer: a token sparsification framework for training and inference acceleration. In *Forty-first International Conference on Machine Learning*, 2024.
- [50] Haiyan Jiang, Giulia De Masi, Huan Xiong, and Bin Gu. Ndot: Neuronal dynamics-based online training for spiking neural networks. In *Forty-first International Conference on Machine Learning*, 2024.

- [51] Yulong Huang, Xiaopeng Lin, Hongwei Ren, Haotian Fu, Yue Zhou, Zunchang Liu, Biao Pan, and Bojun Cheng. Clif: Complementary leaky integrate-and-fire neuron for spiking neural networks. *arXiv preprint arXiv:2402.04663*, 2024.
- [52] Ziming Wang, Runhao Jiang, Shuang Lian, Rui Yan, and Huajin Tang. Adaptive smoothing gradient learning for spiking neural networks. In *International Conference on Machine Learning*, pages 35798–35816. PMLR, 2023.
- [53] Jianhao Ding, Zhaofei Yu, Tiejun Huang, and Jian K Liu. Enhancing the robustness of spiking neural networks with stochastic gating mechanisms. In *Proceedings of the AAAI Conference on Artificial Intelligence*, volume 38, pages 492–502, 2024.
- [54] Wulfram Gerstner and Werner M Kistler. *Spiking neuron models: Single neurons, populations, plasticity*. Cambridge university press, 2002.
- [55] Yujie Wu, Lei Deng, Guoqi Li, Jun Zhu, Yuan Xie, and Luping Shi. Direct training for spiking neural networks: Faster, larger, better. In *Proceedings of the AAAI conference on artificial intelligence*, volume 33, pages 1311–1318, 2019.
- [56] Hanle Zheng, Yujie Wu, Lei Deng, Yifan Hu, and Guoqi Li. Going deeper with directly-trained larger spiking neural networks. In *Proceedings of the AAAI conference on artificial intelligence*, volume 35, pages 11062–11070, 2021.
- [57] Jason K Eshraghian, Max Ward, Emre O Neftci, Xinxin Wang, Gregor Lenz, Girish Dwivedi, Mohammed Bennamoun, Doo Seok Jeong, and Wei D Lu. Training spiking neural networks using lessons from deep learning. *Proceedings of the IEEE*, 111(9):1016–1054, 2023.
- [58] Qingyang Wang, Albert Cardona, Marta Zlatic, Joshua T Vogelstein, and Carey E Priebe. Why do we have so many excitatory neurons? *bioRxiv*, pages 2024–09, 2024.
- [59] Khadeejah T Sultan and Song-Hai Shi. Generation of diverse cortical inhibitory interneurons. *Wiley Interdisciplinary Reviews: Developmental Biology*, 7(2):e306, 2018.
- [60] Greg Brockman, Vicki Cheung, Ludwig Pettersson, Jonas Schneider, John Schulman, Jie Tang, and Wojciech Zaremba. Openai gym, 2016.